Hindawi
Geofluids
Volume 2022, Article ID 9032572, 16 pages
https://doi.org/10.1155/2022/9032572

Research Article

Effect of Water on Mechanical Properties of Coal Measures Mudstone Using Nanoindentation

Wenshuai Li,[1] **Bangyou Jiang**,[2] **and Shitan Gu**[2]

[1]*Shandong Key Laboratory of Civil Engineering Disaster Prevention and Mitigation, Shandong University of Science and Technology, Qingdao 266590, China*
[2]*College of Energy and Mining Engineering, Shandong University of Science and Technology, Qingdao 266590, China*

Correspondence should be addressed to Bangyou Jiang; jiangbangyou123@163.com and Shitan Gu; chinasdgst@163.com

Received 15 September 2021; Revised 26 February 2022; Accepted 5 March 2022; Published 6 May 2022

Academic Editor: Andrea Brogi

Mudstone rich in clay minerals exhibits an obvious water-induced weakening effect, and the mechanical properties of mudstone are significantly affected by the groundwater. To investigate the effect of water on mechanical characteristics of mudstone at microscale, a series of uniaxial compression and nanoindentation tests were conducted on mudstone specimens at different moisture contents. Microscale measurements are upscaled to estimate the corresponding magnitudes at the macroscale using the Mori-Tanaka method. The results showed that the indentation modulus varied significantly, from as low as 0.2 GPa to a quite high value of 125 GPa, indicating a strongly heterogeneous distribution of mudstone. The water illustrated a significant effect on the microscale mechanical properties of water-sensitivity minerals like clay minerals. The water-sensitivity minerals occupied the highest proportion of the mudstone and were believed to play an important role in the mechanical properties of mudstone. For water-bearing specimens, the comparison with elastic modulus data obtained from common method indicated similar values as those predicted by homogenization method. The results of this study indicated that nanoindentation technique is a feasible experimental technique to assess the macroscale mechanical properties of rock materials.

1. Introduction

In China, about 60% of identified coal reserves are located at depth of more than 800 m and about 53% at depth below 1000 m [1–3]. The deep roadways are often excavated in sedimentary rocks near the coal seams [4, 5], such as mudstone. For decades, most research has been focused on the mechanical properties of coal measures rocks, including strength, deformation, and failure characteristics [6–10]. Due to the heterogeneity of coal measures rocks, it is thus vital to understand the mechanical characteristics at microscale [11, 12].

Nowadays, nanoindentation is used to investigate the microscale mechanical properties of rocks. Nanoindentation is based on elastic contact theory allowing obtaining the mechanical parameters at microscale, such as indentation modulus and hardness. Oliver and Pharr [13] established an improved method to determine the modulus and hardness from nanoindentation load-depth curves, which has been widely used in rock-like materials [14, 15]. Afterward, many researchers studied the microscale mechanical properties (*e.g.*, deformation, modulus, and hardness) of coal [16–19], shale [20], and cement-based materials [21–24]. Furthermore, Scanning Electron Microscopy (SEM) and Atomic Force Microscope (AFM) were also used to investigate nanoscale detection of the pore distribution and mechanical properties of rock [25, 26]. With large numbers of indents that carried out on the specimen surface, the mechanical properties of material can be obtained exclusively. However, previous studies have mainly focused on the field of oil and gas exploitation (such as shale and coal) or construction materials. By contrast, the microscale mechanical properties of coal measures mudstone are still not fully understood [19].

Furthermore, the mechanical properties of coal measures mudstone do not only depend on mineral components but are significantly affected by the external environment, especially the groundwater [27–30]. Mudstone rich in clay

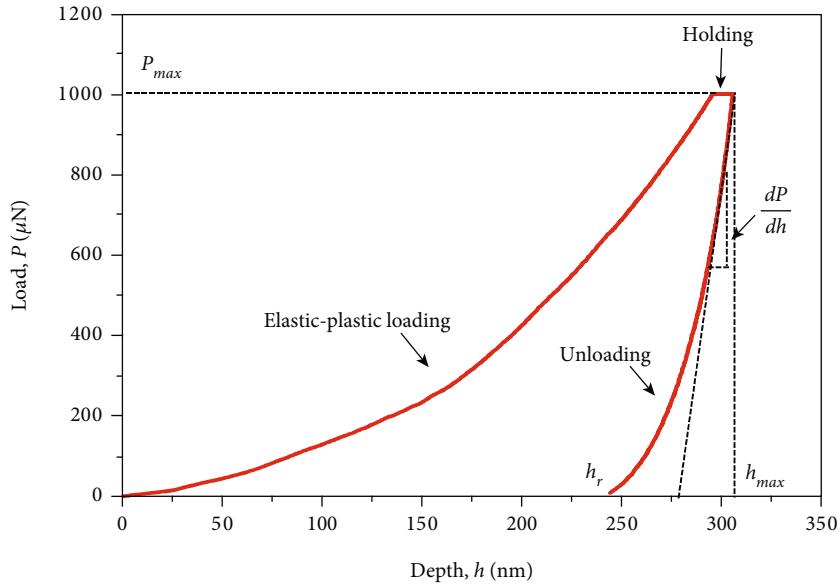

Figure 1: Typical load-depth curve obtained from nanoindentation.

Figure 2: Sampling location map in Anhui, eastern China.

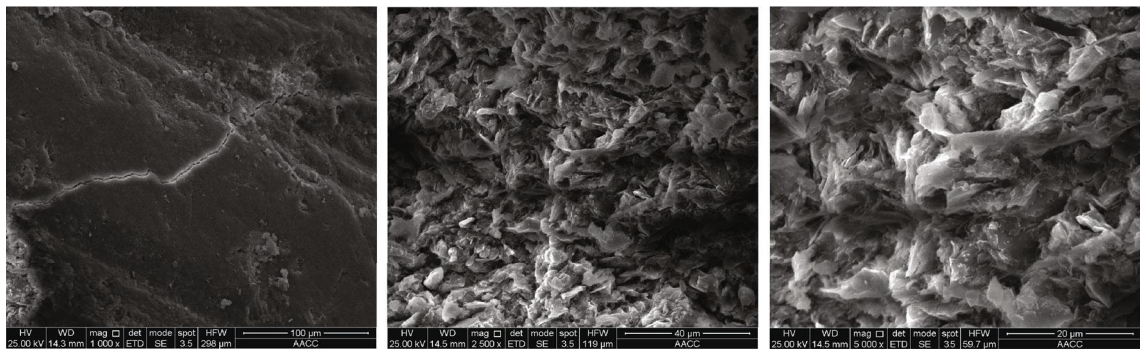

Figure 3: SEM photomicrographs of mudstone.

Table 1: Experimental scheme.

Uniaxial compressive test	Nanoindentation	Moisture content (%)
M-1	NM-1	~0.0
M-2	NM-2	~2.4
M-3	NM-3	~6.4

minerals exhibits an obvious water-induced weakening effect [31], and the increase in moisture content usually reduces the strength of rock [32]. However, due to the water sensitivity of argillite, it is generally a delicate task to investigate the mechanical properties in high moisture content mudstone by the specimens with standard size by bulk measurements (*e.g.*, acoustic emission, uniaxial compression, triaxial compression, and direct shear test) in some engineering fields. Thus, nanoindentation is a feasible experimental technique allowing for assessment of the mechanical properties of rock materials.

To the best of our knowledge, studies related to the effect of water on the microscale mechanical properties of coal measures mudstone are still lacking. Hence, nanoindentation was adopted to investigate the microscale mechanical properties of mudstone in this work. The effects of water on micro mechanical properties were analyzed, and the results were discussed.

2. Theory and Background

The principle of nanoindentation consisted of making contact between an indenter tip and the material surface. The changes in the applied load and penetration depth were measured simultaneously [33–35]. A typical indentation load-depth curve is shown in Figure 1. It consisted of three stages: loading, holding, and unloading. During the loading stage, the load increased as a function of the penetration depth, regarded as elastic-plastic loading. In the unloading stage, only elastic deformation was recovered and used to calculate the microscale mechanical properties of the specimen [36]. In Figure 1, $P_{\max}$ is the peak indentation load, $h_{\max}$ refers to the indentation depth at peak load, and h_f is the final depth of the contact impression after unloading.

From the load-depth curve, the initial unloading stiffness (S) can be expressed by Equation (1) [13].

$$S = \frac{dP}{dh} = \frac{2}{\sqrt{\pi}} \left(\frac{1}{E_r}\right)^{-1} \sqrt{A_c}, \tag{1}$$

where P is indentation load, h denotes the indentation depth, A_c is contact area of indenter at peak load, and E_r refers to the reduced modulus that can be determined by Equation (2).

$$\frac{1}{E_r} = \frac{1\text{-}\nu^2}{E} + \frac{1\text{-}\nu_i^2}{E_i}, \tag{2}$$

where E and ν are Young's modulus and Poisson's ratio of specimen, respectively. E_i and ν_i are Young's modulus and Poisson's ratio of indenter, respectively. A common Berkovich indenter was used in the present study, with Young's modulus $E_i = 1140$ GPa and Poisson's ratio $\nu_i = 0.07$.

Based on the principles of elastic contact theory, the modulus and hardness (H) of mudstone specimen can be calculated according to Equations (3) and (4).

$$E = \left(1\text{-}\nu^2\right)\left[\frac{1}{E_r} - \frac{1\text{-}\nu_i^2}{E_i}\right]^{-1}, \tag{3}$$

$$H = \frac{P_{\max}}{A_c}. \tag{4}$$

3. Experimental Material and Methods

3.1. Specimen Preparation. The mudstone was collected from the floor strata of a coal seam in Kouzidong coal mine located at Anhui in eastern China. Figure 2 shows the location where the mudstone was found. Figure 3 illustrates the SEM photomicrographs of the tested mudstone specimens. Loosed thin sheets were observed in the microstructure of the mudstone. According to the XRD results, the main mineral components of the mudstone were made of kaolinite (~52.2%), illite (~12.3%), chlorite (~28.1%), and quartz (~7.4%).

For uniaxial compression testing, the mudstone was cut into a series of cylindrical specimens with 50 mm in diameter and 100 mm in height. All specimens were fabricated from a large block of mudstone. The ends of the finished specimens were adjusted with a surface grinder to ensure nonparallelism and nonperpendicularity both less than 0.02 mm. The prepared specimens were tested by ultrasonic velocity measurements to select homogeneous specimens. In this study, specimens with three different moisture contents were prepared and the experimental scheme is summarized in Table 1. Three tests were repeated for each condition to minimize the dispersion of test results caused by the heterogeneity of the specimen.

After uniaxial compression tests, broken pieces were collected from the fractured specimens to prepare the specimens for nanoindentation, as shown in Table 1. For nanoindentation, it was based on the assumption of a perfectly smooth material surface since the smoothness was very important in obtaining reliable nanoindentation data [37, 38]. Before nanoindentation, the specimens were carefully ground and polished to achieve a smooth surface. The specimens were then cast in epoxy resin to create total stability for grinding and polishing during surface preparation. After solidification for 24 h, the specimens were ground using a grinder-polisher machine. An initial grinding and polishing of specimens were then conducted on silicon carbide papers with reduced gradation 52 μm, 35 μm, 22 μm, and 15 μm to expose the surface of each specimen. Preparation of specimens was completed after the final stage of grinding and polishing by diamond suspension with decreased size of 9 μm, 6 μm, 3 μm, 1 μm, and 0.05 μm on a polishing cloth. To avoid further change in the moisture content of mudstone, methanol-based liquids were used as

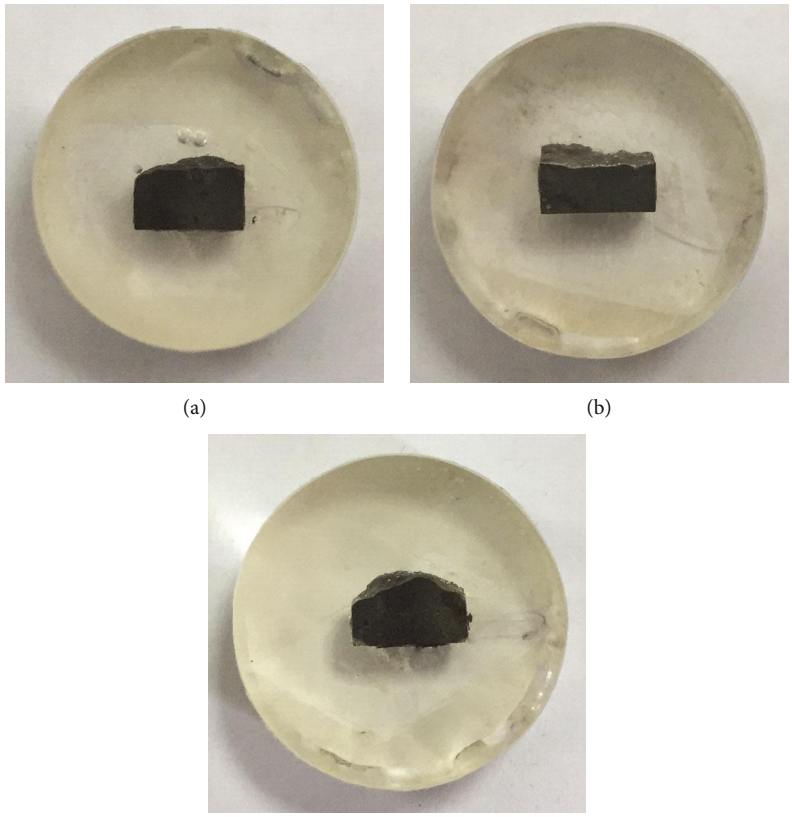

(a) (b) (c)

Figure 4: Well-prepared specimens: (a) NM-1, (b) NM-2, and (c) NM-3.

lubricants in the polishing process. The well-prepared specimens with smooth and flat surfaces used for nanoindentation are shown in Figure 4.

3.2. Nanoindentation. After polishing the specimens, a Hysitron T1 Premier (Figure 5) was used to investigate the microscale mechanical characteristics of all three mudstone specimens. A representative area of $100\,\mu m \times 100\,\mu m$ was selected for nanoindentation, as shown in Figure 6. A matrix of 100 indents was made on the surface, whereas the indent spacing was kept to $10\,\mu m$ in the vertical and lateral directions (Figure 6). In this study, a load control mode was adopted, and tests were programmed in such a way that the indenter came in contact with the specimen surface. Afterward, the load was increased at a constant rate of $200\,\mu N/s$ until reaching a maximum load value of $1000\,\mu N$. For the tested point, the maximum load of 1.0 mN here was determined so to respect on-average the scale separability condition and the 1/10 rule of thumb [39]. Next, the load was held at its maximum value for 2 s at the same loading rate before unloading to minimize the short-term creep and size effect [40, 41]. The movement protocol from one indent to the next was set as a constant direction mode. The unloading data were used to determine the indentation modulus and hardness values based on well-established equations.

Figure 5: Hysitron T1 Premier.

3.3. Statistical Analysis. The experimental data obtained by nanoindentation were used to estimate the elastic properties of different phases of mudstone specimens. Using a statistical Gaussian fitting method [14, 15, 42, 43], the microscale

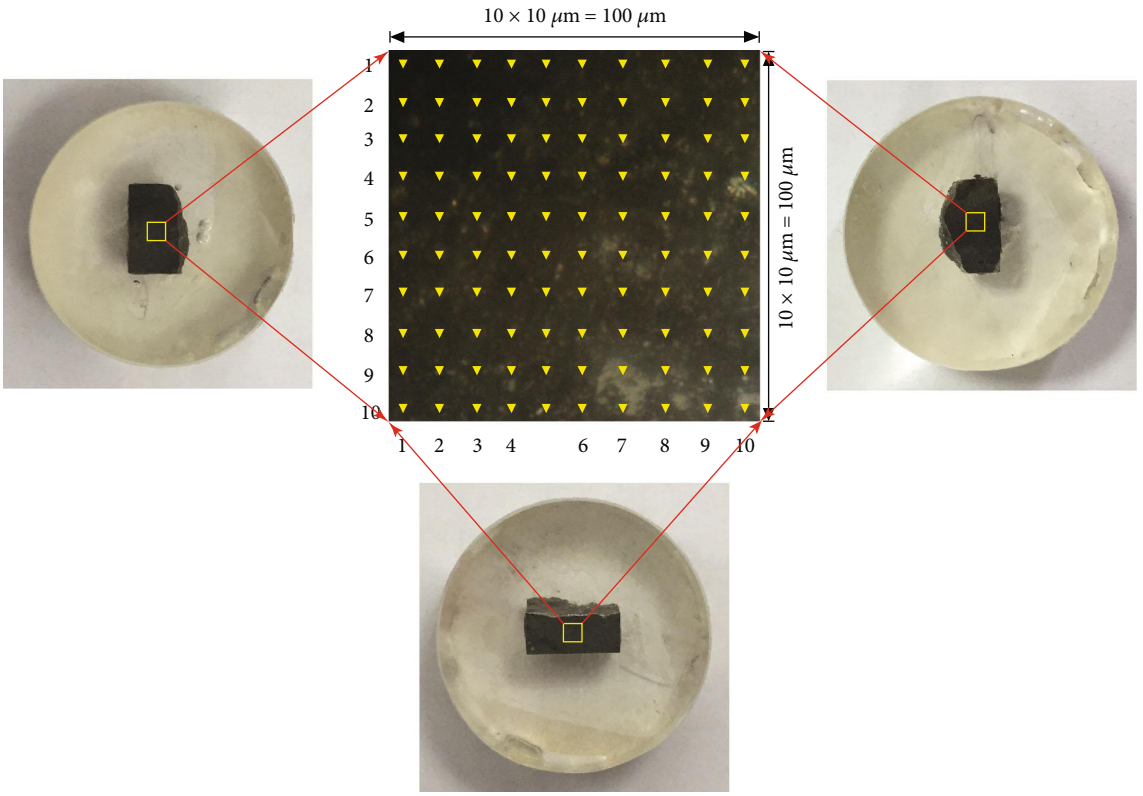

Figure 6: Indent arrangement on mudstone surface.

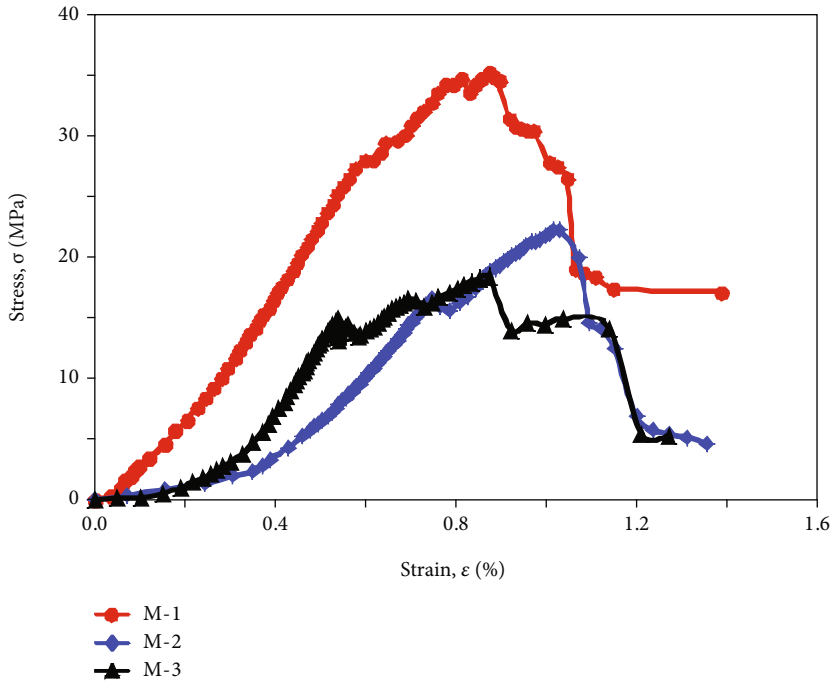

Figure 7: Uniaxial compression stress-strain curves of mudstone specimens: (a) M-1, (b) M-2, and (c) M-3.

Table 2: Mechanical properties of mudstone.

Rock types	Uniaxial compressive strength (MPa)		Young's modulus (GPa)	
	Experimental	Average	Experimental	Average
M-1	34.8	34.7	5.7	6.1
	34.8		5.6	
	34.6		6.9	
M-2	21.8	22.5	3.8	4.3
	24.1		4.9	
	21.7		4.2	
M-3	18.4	18.6	5.5	4.1
	17.8		3.6	
	19.6		3.2	

mechanical properties of different phases were analyzed statistically. The best model based on multimodal normal distribution curves (Gaussian distribution) was used to fit the experimental results following Equation (5).

$$f(x, \mu, \sigma) = \frac{1}{\sigma\sqrt{2\pi}} \exp\left[-\frac{(x-\mu)^2}{2\sigma^2}\right]. \quad (5)$$

The mean value μ and standard deviation σ of distribution can be extracted from each model fitting. When the number and distribution type of phases comprising a composite are known, the volume fraction for different phases can be estimated by the area under the normal distribution curve [15, 44].

4. Results and Discussion

4.1. Mechanical Behavior of Mudstone at Macroscale. The uniaxial compression tests were performed on mudstone specimens with different moisture contents, and typical stress-strain curves of the three specimens are shown in Figure 7. All three types of mudstone specimens exhibited similar mechanical behaviors. The values of uniaxial compressive strength and Young's modulus of different specimens are summarized in Table 2. Compared to specimen M-1, the average uniaxial compression strength of specimens M-2 and M-3 decreased by 35.2% and 46.4%, and Young's modulus declined by approximately 29.5% and 32.8%, respectively. Due to the water-weakening effect, the macroscale mechanical properties significantly decreased.

4.2. Nanoindentation Load-Depth Curves. To investigate the mechanical properties of mudstone at microscale, Figure 8 shows the typical load-depth curves of indented points in the tested areas of all three mudstone specimens. As shown in Figure 8, each loading and unloading cycle illustrated a deformation behavior of mudstone around the indented point.

The visual inspection of the load-depth curves revealed large differences in final depth values at the end of loading. Such different characteristic shapes represented the mechanical responses of various types of minerals induced by the heterogeneousity of mudstone. At the same maximum load (1000 μN), the final depths of left-most curves were much lower than in other curves, indicating strong resistance to external stress due to the existence of hard mineral grains in mudstone. The right-most curves with the largest final depth and clear creeping branch represented typical responses on the weakest mineral grains. When the maximum load was maintained for 2 s, the creep deformation of mudstone at the right-most curves was much larger than in left-most curves. Furthermore, the final depth of most curves observed from the mudstone specimens increased as a function of moisture content (Figure 8).

4.3. Mechanical Mapping of Indentation Modulus and Hardness. The indentation modulus and hardness of different tested points were calculated from the obtained load-depth curves using the Oliver-Pharr method. Figures 9–11 show the distribution of the indentation modulus and hardness in tested regions of three mudstone specimens. The color difference in the tested regions indicated a relatively complex and highly heterogeneous composition of mudstone. The blue area showing the lower modulus (hardness) represented the weak zones in mudstone, whereas the red area with a significantly higher modulus (hardness) displayed the rigid part. The other areas with the modulus (hardness) between the weak zones (shown in blue) and rigid part (shown in red) were exhibited in green or yellow. The elastic modulus of tested points in mudstone varied significantly, indicating a strongly heterogeneous distribution. This was caused by different mineral components in the rocks.

The general comparison of the mechanical properties maps (indentation modulus and hardness) showed considerable variations in different mudstone specimens. For specimen NM-1, the red area with higher indentation modulus accounted for a large proportion (Figure 9(a)) but decreased in specimens NM-2 (Figure 10(a)) and NM-3 (Figure 11(a)). Furthermore, the red area with highest modulus (100-120 GPa) still existed after water adsorption (Figure 11(a)).

Additionally, the tested points with higher indentation moduli corresponded to the elevated hardness values (Figures 9–11). The distribution map of indentation modulus and hardness looked similar in appearance. The correlation between indentation modulus and hardness of the three mudstone specimens is shown in Figure 12. The correlation between indentation modulus and hardness varied linearly with a positive slope.

4.4. Microcharacterization of Multiphase Structure in Mudstone. In multiphase (multimineral) materials like mudstone, nanoindentation could provide approximate information related to the microscale of each phase, as well as the role in the effective properties of multiphase systems [16]. Here, the contact surface area was around a few square microns, and different phases can be identified at a much finer scale. To distinguish different phases, Figure 13 shows a histogram of indentation moduli of different tested points in the three mudstone specimens. The distribution of

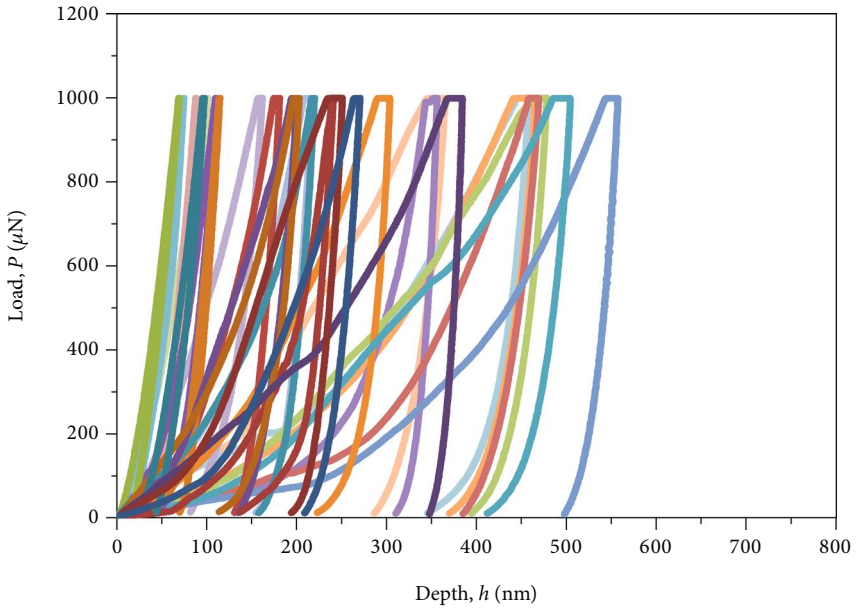

(a)

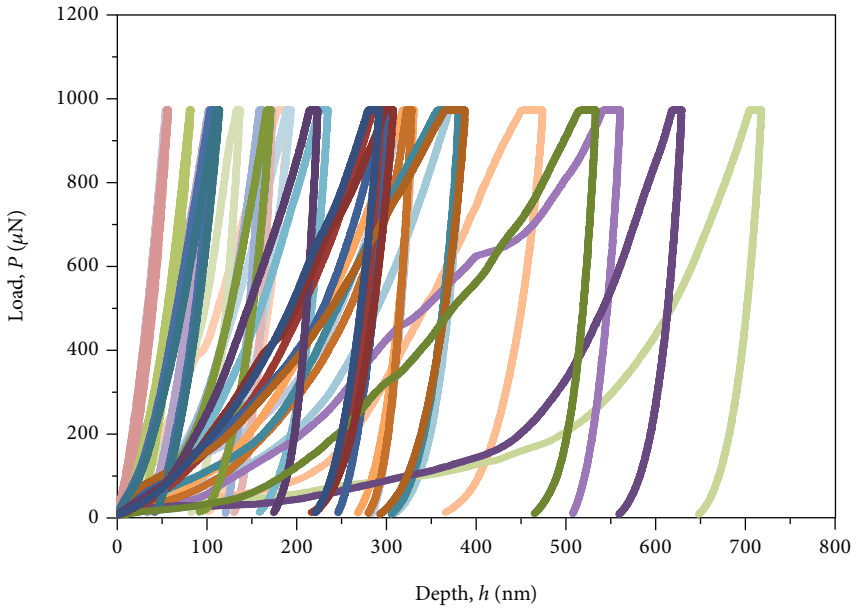

(b)

Figure 8: Continued.

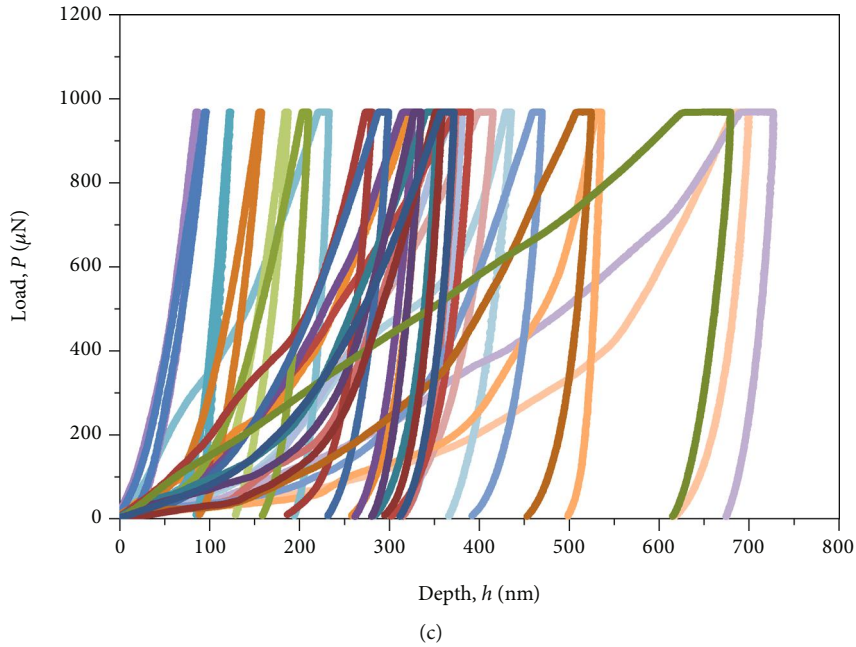

(c)

Figure 8: Typical load-depth curves of mudstone specimens obtained from nanoindentation: (a) NM-1, (b) NM-2, and (c) NM-3.

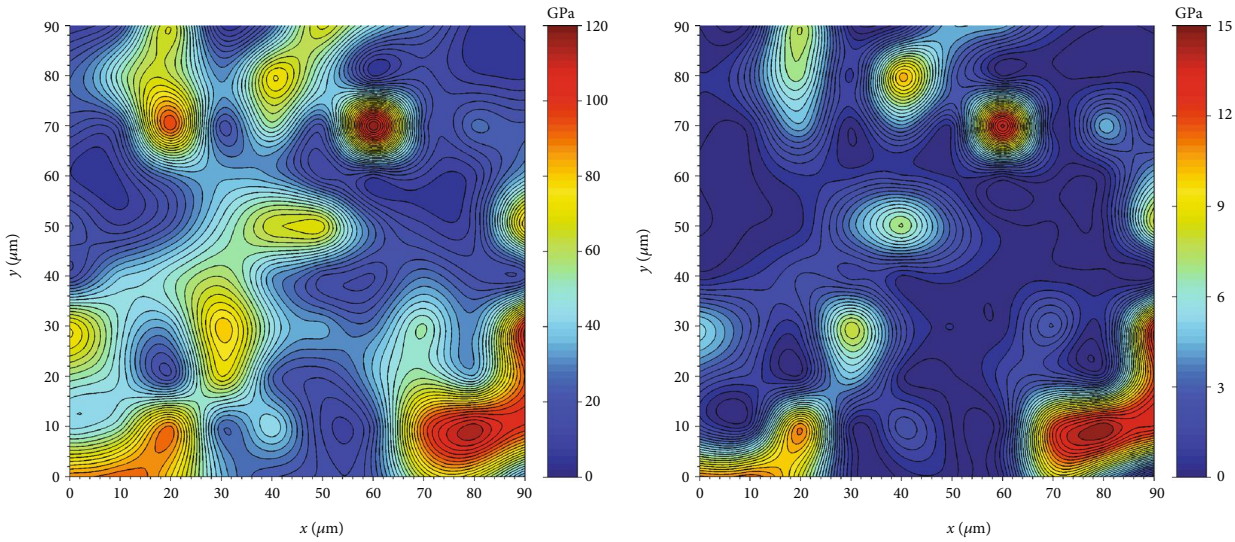

(a) (b)

Figure 9: Distribution of (a) indentation modulus and (b) hardness in the tested region of specimen NM-1.

indentation modulus was in a wide range from 0.2 GPa to 125 GPa. More than one peak can be observed in the indentation modulus histogram, indicating relatively heterogeneous characteristics. For each specimen, the indentation modulus concentrated on 0-60 GPa occupied the highest proportion.

For specimen NM-2 (Figure 13(b)), the frequency increased firstly with the increase in modulus from 0 GPa, until it reached a peak value between 3 GPa and 9 GPa. Afterward, the frequency decreased from 9 to 24 GPa. Note that the frequency between 0 and 24 GPa accounted for the largest proportion of 75.0%. As the modulus increased from 24 GPa to 63 GPa, the frequency exhibited an initial increase followed by a decrease. The modulus in the range of 24-63 GPa accounted for 16.0%. After a large discontinuity (63-84 GPa), the frequency of modulus at 84-115 GPa reached 9.0%.

After drying, the frequency distribution of indentation modulus of NM-1 (Figure 13(a)) was different from that of NM-2 and looked more uniform. The frequency of modulus at 5-45 GPa, 45-80 GPa, and 80-130 GPa was 62.0%, 25.0%, and 13.0%, respectively. For specimen NM-3 (Figure 13(c)), the frequency distribution of modulus was similar to that of specimen NM-2.

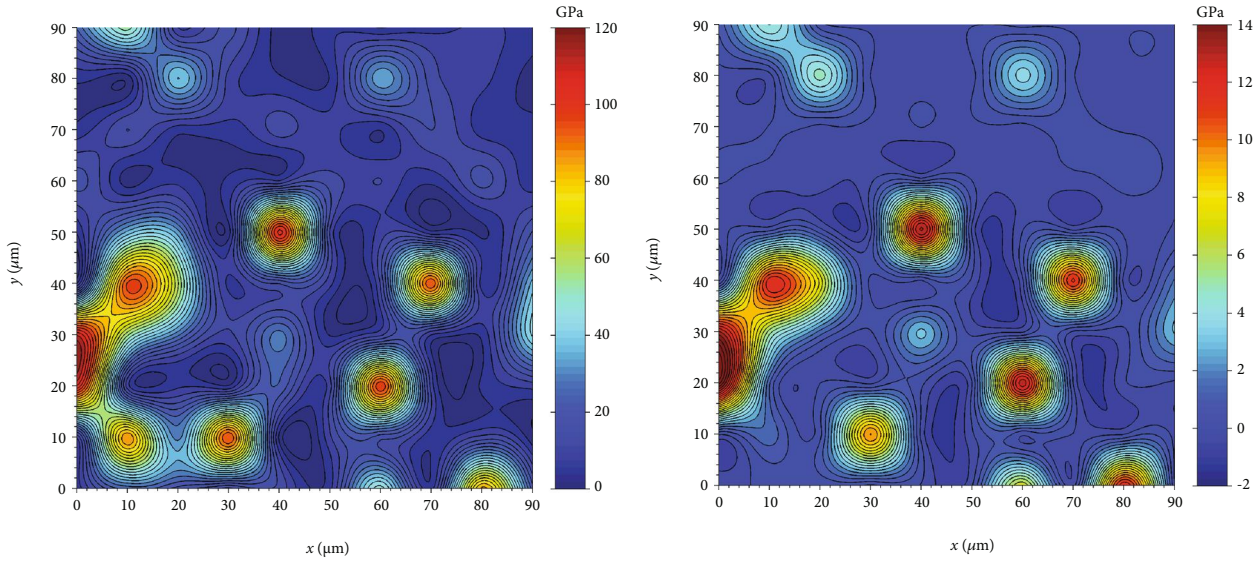

Figure 10: Distribution of (a) indentation modulus and (b) hardness in the tested region of specimen NM-2.

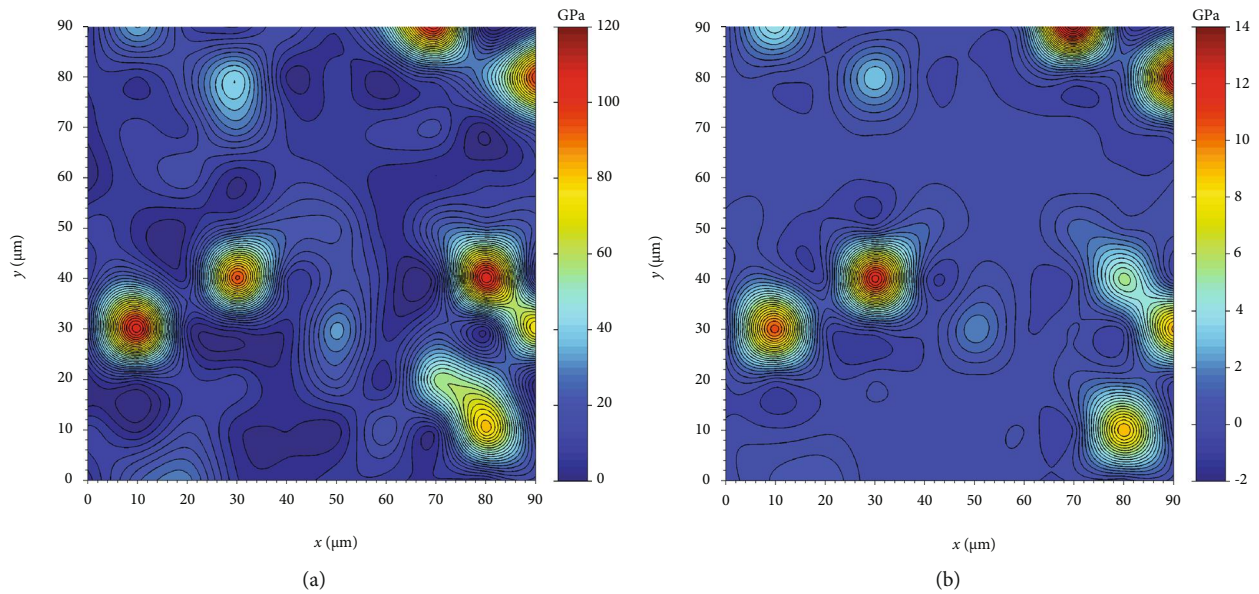

Figure 11: Distribution of (a) indentation modulus and (b) hardness in the tested region of specimen NM-3.

4.5. Effect of Water on Microscale Mechanical Properties of Phases. In terms of microscale characterization, mudstone is a material composed of different phases. To further investigate the effects of moisture contents on the mechanical properties of mudstone specimens at microscale, Gaussian fitting was used to analyze the statistical results of mechanical properties. Figure 14 shows the experimental data and fractions of each Gaussian probability density of indentation modulus of all three mudstone specimens. In each figure, three model normal distribution curves were used to produce the best fit of the experimental data. Table 3 summarizes the modulus values extracted from the model fits of individual phases in different mudstone specimens. The volume fractions of different phases were also included in Table 3.

For clay minerals (kaolinite, etc.), Zhang et al. [45] reported that the modulus was less than 5.0 GPa in claystone, while Liu et al. [36] reported it was 22.3 GPa. Our results showed that indentation moduli of clay minerals (including kaolinite and illite) were in a range from 4.2 to 17.7 GPa. This difference in indentation moduli of clay minerals obtained from different studies may be caused by variable moisture contents in the specimens, and an explanation of this variation in indentation modulus values of clay minerals was the water-weakening effect or swelling effect, as previously reported [28, 46, 47].

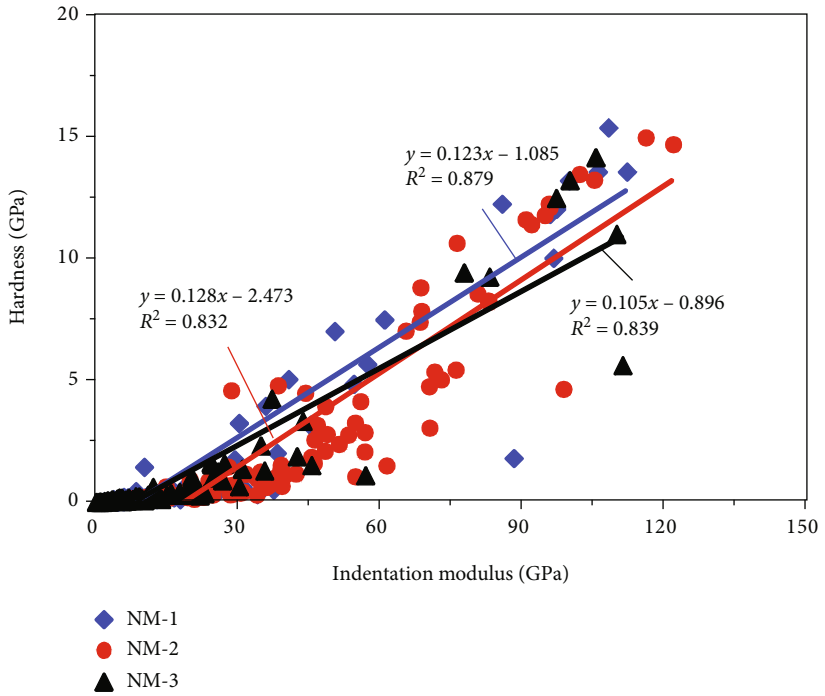

Figure 12: Correlation between indentation modulus and hardness of all three mudstone specimens.

From Table 3, it was apparent that the variation in indentation modulus looked relatively different for the dry specimen (NM-1) and water-bearing specimens (NM-2 and NM-3). For the same mineral composition (*e.g.*, clay minerals), the indentation modulus in NM-1 was larger than that in specimens NM-2 and NM-3. The swelling effect reduced the indentation modulus of kaolinite in specimen NM-2 to 4.67 GPa, while 17.68 GPa was recorded for specimen NM-1. With the increase in moisture content, the modulus of kaolinite decreased to 4.22 GPa (NM-3). Compared to the dry specimen (NM-1), the indentation moduli of kaolinite in specimens NM-2 and NM-3 decreased by approximately 73.6% and 76.1%, respectively. Also, the indentation moduli of chlorite diminished by approximately 39.8% and 52.1%, respectively. The difference in moisture content of all three mudstones led to variable mechanical properties of clay minerals (kaolinite, illite, and chlorite) at microscale.

The volume fractions of different phases were also analyzed. As shown in Table 3, the volumes of water-sensibility minerals of specimen NM-1 were estimated to 58.3% (kaolinite, etc.) and 27.2% (chlorite), respectively. By comparison, values of 80.7% (kaolinite, etc.) and 13.2% (chlorite) were obtained for specimen NM-2 and 77.7% and 18.0% for specimen NM-3, respectively.

For hard minerals (quartz), the indentation modulus of quartz ranged from 87 to 105 GPa. Zhu et al. [15] reported that the modulus of quartz in quartzite was 104.2 ± 5.9 GPa. Thus, the values for quartz determined in this study were reasonable. Compared to dry specimen NM-1, the statistical results of indentation modulus of quartz in specimens NM-2 and NM-3 increased by 11.0% and 18.6%, respectively.

Note that the indentation modulus may not represent the exact values for the pure phase due to unavoidable phase interactions. For example, the reported modulus of a specially prepared pure phase of quartz by nanoindentation was 117.26 ± 2.7 GPa [48]. This value was higher than those obtained in the present study or other reported ones [15, 36, 45]. Clearly, the complete separation of the mechanical performances of different individual phases was not possible from the measurement response. Though the characterization results were based on mechanically distinct phases instead of pure chemically distinct phases, they looked very well related.

4.6. Mechanical Properties at Macro- and Microscale. The average moduli obtained from uniaxial compression and nanoindentation tests were compared in Figure 15. The average moduli at macro- and microscale varied significantly, and the values obtained from nanoindentation looked much larger than those from macroscopic experiments. Compared to nanoindentation, the average modulus obtained from uniaxial compression tests decreased by approximately 80.0%.

The diversity in microscale mechanical properties of different phases rendered the average nanoindentation modulus unsuitable for characterizing the mechanical properties of specimens at macroscale. Therefore, the Mori-Tanaka method was used to link the nanoindentation data and macroscopic mechanical properties [49]. Based on homogenization scheme and nanoindentation data, Zhang et al. [45] and Liu et al. [36] determined the elastic properties of claystone and shale, respectively. The comparison with modulus data obtained from common method indicated similar values as those predicted by homogenization method.

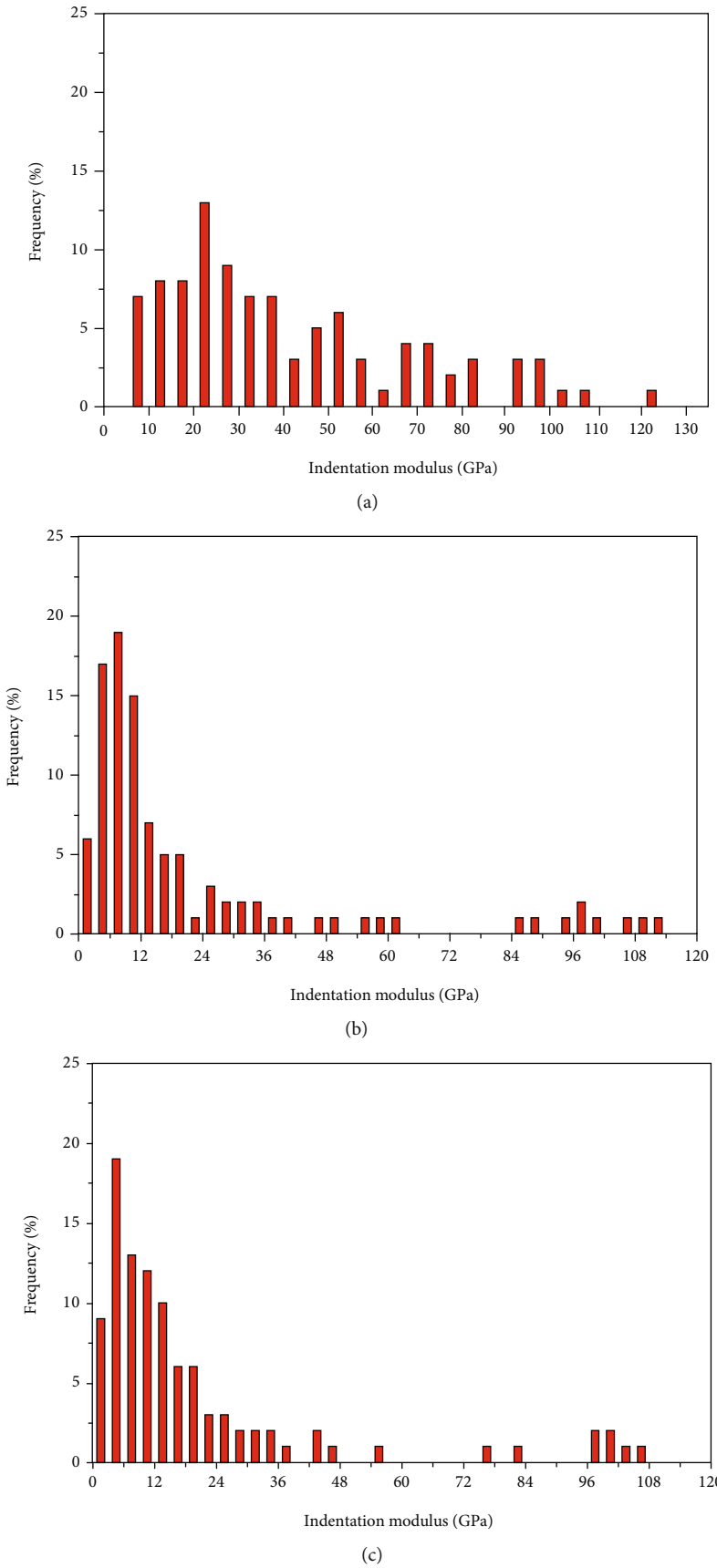

Figure 13: Histograms of indentation modulus of (a) NM-1, (b) NM-2, and (c) NM-3.

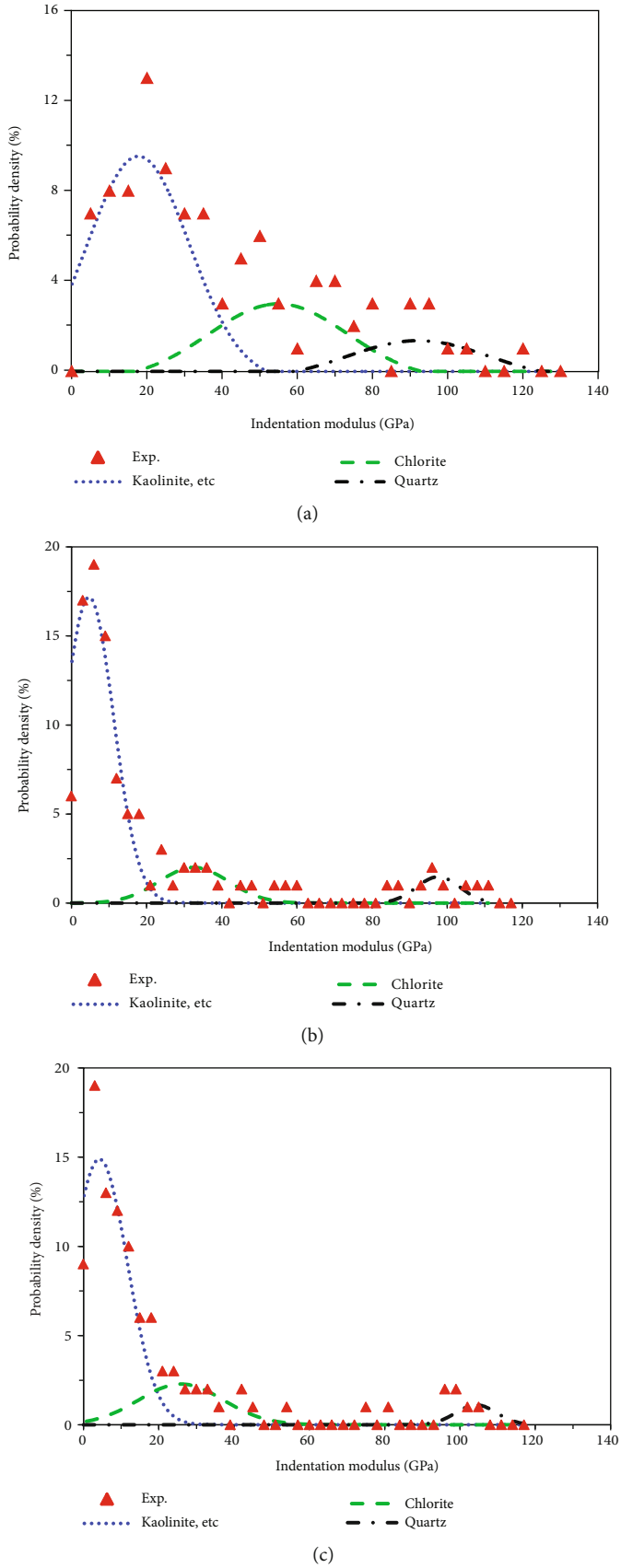

Figure 14: Fractions of each Gaussian probability density of indentation modulus of (a) NM-1, (b) NM-2, and (c) NM-3.

Table 3: Statistical results of indentation modulus for three mudstone specimens.

Rock types	Kaolinite, etc.		Chlorite		Quartz	
	Modulus (GPa)	V (%)	Modulus (GPa)	V (%)	Modulus (GPa)	V (%)
NM-1	17.68	58.3	54.08	27.2	87.96	14.5
NM-2	4.67	80.7	32.56	13.2	97.62	6.1
NM-3	4.22	77.7	25.90	18.0	104.30	4.3

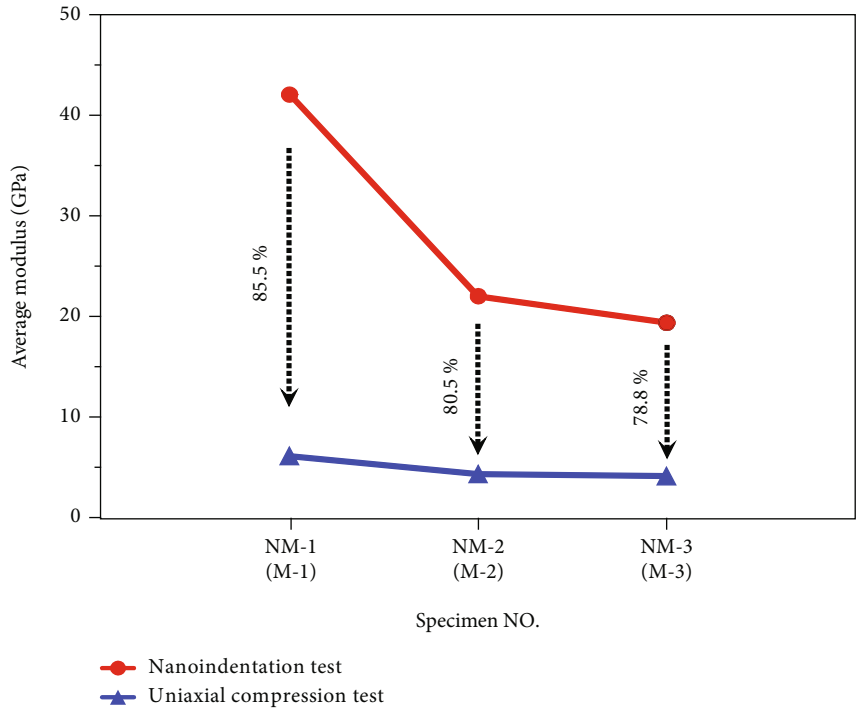

Figure 15: Comparison of average modulus of all specimens obtained from uniaxial compression and nanoindentation tests.

Table 4: Test results of homogenization and macroscopic experiments.

Rock types	Phases Name	E (GPa)	ν	V (%)	E_{macro} (GPa)	E_{micro} (GPa)	E_{hom} (GPa)	Error (%)
NM-1	Kaolinite, etc.	17.68	0.30	58.3	6.1	42.2	28.7	370.5
	Chlorite	54.08	0.25	27.2				
	Quartz	87.96	0.20	14.5				
NM-2	Kaolinite, etc.	4.67	0.30	80.7	4.3	22.0	6.4	48.8
	Chlorite	32.56	0.25	13.2				
	Quartz	97.62	0.20	6.1				
NM-3	Kaolinite, etc.	4.22	0.30	77.7	4.1	19.4	5.9	43.9
	Chlorite	25.90	0.25	18.0				
	Quartz	104.30	0.20	4.3				

Note: Error% = $(E_{hom} - E_{macro})/E_{macro}$.

In this study, linkages of the nanoindentation data and macroscopic mechanical properties were evaluated by homogenization scheme. Table 4 shows the input parameters of different phases of three specimens, as well as the homogenized elastic modulus (E_{hom}) values obtained by Mori-Tanaka method. The macroscopic experimental results (E_{macro}) and average indentation modulus (E_{micro}) were also included in Table 4. The Poisson's ratios associated with the clay minerals and quartz were obtained from literature [36, 45].

As shown in Table 4, the errors between the results obtained from the uniaxial compression test and

homogenization method were estimated to about 45.0% for water-bearing specimens (NM-2 and NM-3). The evaluating results seemed reasonable, while for dry specimen of NM-1, the error was 370.5%. It seemed that the homogenization scheme cannot upscale the microscale mechanical properties of different phases to obtain data of the whole specimen at macroscale in dry specimen. After drying, the mechanical properties of water-sensitivity minerals increased significantly (Figure 13(a)), and the input parameters (Table 4) of different phases for dry specimens may not represent the actual value.

5. Conclusions

In this study, the effects of moisture contents on the macro- and microscale mechanical properties of mudstone were analyzed and the results were discussed. The following conclusions can be drawn:

(1) The load-depth curves, curve-based indentation modulus, and hardness were all obtained. The indentation modulus varied significantly from a low value of 0.2 GPa to a high value of 125 GPa, demonstrating a strongly heterogeneous distribution of different minerals in mudstone

(2) The moisture content showed a significant effect on the microscale mechanical properties of water-sensitivity minerals. The water-sensitivity minerals occupying the highest proportion of mudstone played a decisive role in the mechanical properties of mudstone

(3) The average moduli at macro- and microscale varied significantly, and the average elastic modulus values obtained from nanoindentation were much larger than those acquired by macroscopic experiments. The Mori-Tanaka method was used to link the nanoindentation data and macroscopic mechanical properties. The results of this study indicated that nanoindentation technique is a feasible experimental technique to assess the macroscale mechanical properties of rock materials

Data Availability

The data used to support the finding of this study are available from the corresponding author upon request.

Conflicts of Interest

The authors declare that there are no conflicts of interest.

Acknowledgments

This research is supported by the Natural Science Foundation of China (52004144), the Natural Science Foundation of Shandong Province, China (ZR2019BEE001), and the Project of Shandong Province Higher Educational Young Innovative Talent Introduction and Cultivation Team (Disaster prevention and control team of underground engineering involved in sea).

References

[1] Y. L. Lu, L. G. Wang, X. K. Sun, and J. Wang, "Experimental study of the influence of water and temperature on the mechanical behavior of mudstone and sandstone," *Bulletin of Engineering Geology and the Environment*, vol. 76, no. 2, pp. 645–660, 2017.

[2] S. Tao, S. D. Chen, and Z. J. Pan, "Current status, challenges, and policy suggestions for coalbed methane industry development in China: a review," *Energy Science & Engineering*, vol. 7, no. 4, pp. 1059–1074, 2019.

[3] S. Tao, Z. J. Pan, S. L. Tang, and S. D. Chen, "Current status and geological conditions for the applicability of CBM drilling technologies in China: a review," *International Journal of Coal Geology*, vol. 202, pp. 95–108, 2019.

[4] Y. Li, J. H. Yang, Z. J. Pan, S. Z. Meng, K. Wang, and X. L. Niu, "Unconventional natural gas accumulations in stacked deposits: a discussion of upper Paleozoic coal-bearing strata in the east margin of the Ordos Basin, China," *Acta Geologica Sinica-english Edition*, vol. 93, no. 1, pp. 111–129, 2019.

[5] Y. Li, D. Z. Tang, P. Wu et al., "Continuous unconventional natural gas accumulations of Carboniferous-Permian coal-bearing strata in the Linxing area, northeastern Ordos Basin, China," *Journal of Natural Gas Science and Engineering*, vol. 36, pp. 314–327, 2016.

[6] B. Y. Jiang, S. T. Gu, G. C. Zhang, and W. S. Li, "Strainburst process of marble in tunnel-excavation-induced stress path considering intermediate principal stress," *Journal of Central South University*, vol. 26, no. 4, pp. 984–999, 2019.

[7] M. Nicksiar and C. D. Martin, "Crack initiation stress in low porosity crystalline and sedimentary rocks," *Engineering Geology*, vol. 154, no. 2, pp. 64–76, 2013.

[8] M. Li, X. B. Mao, L. L. Cao, H. Pu, R. R. Mao, and A. H. Lu, "Effects of thermal treatment on the dynamic mechanical properties of coal measures sandstone," *Rock Mechanics and Rock Engineering*, vol. 49, no. 9, pp. 3525–3539, 2016.

[9] J. Ye, S. Tao, S. Zhao, S. Li, S. Chen, and Y. Cui, "Characteristics of methane adsorption/desorption heat and energy with respect to coal rank," *Journal of Natural Gas Science and Engineering*, vol. 99, p. 104445, 2022.

[10] Q. Feng, J. C. Jin, S. Zhang, W. W. Liu, X. X. Yang, and W. T. Li, "Study on a damage model and uniaxial compression simulation method of frozen-thawed rock," *Rock Mechanics and Rock Engineering*, vol. 55, no. 1, pp. 187–211, 2022.

[11] O. K. Mahabadi, B. S. A. Tatone, and G. Grasselli, "Influence of microscale heterogeneity and microstructure on the tensile behavior of crystalline rocks," *Journal of Geophysical Research Solid Earth*, vol. 119, no. 7, pp. 5324–5341, 2014.

[12] C. L. Sun, G. C. Li, M. E. Gomah, J. H. Xu, and H. Y. Rong, "Meso-scale mechanical properties of mudstone investigated by nanoindentation," *Engineering Fracture Mechanics*, vol. 238, p. 107245, 2020.

[13] W. C. Oliver and G. M. Pharr, "An improved technique for determining hardness and elastic modulus using load and displacement sensing indentation experiments," *Journal of Materials Research*, vol. 7, no. 6, pp. 1564–1583, 1992.

[14] G. Constantinides and F.-J. Ulm, "The effect of two types of CSH on the elasticity of cement-based materials: results from

nanoindentation and micromechanical modeling," *Cement and Concrete Research*, vol. 34, no. 1, pp. 67–80, 2004.

[15] W. Z. Zhu, J. J. Hughes, N. Bicanic, and C. J. Pearce, "Nanoindentation mapping of mechanical properties of cement paste and natural rocks," *Materials Characterization*, vol. 58, no. 11-12, pp. 1189–1198, 2007.

[16] G. Manjunath and B. Jha, "Nanoscale fracture mechanics of Gondwana coal," *International Journal of Coal Geology*, vol. 204, pp. 102–112, 2019.

[17] Y. H. Zhang, M. Lebedev, A. Al-Yaseri, H. Y. Yu, X. M. Xu, and S. Iglauer, "Characterization of nanoscale rockmechanical properties and microstructures of a Chinese sub-bituminous coal," *Journal of Natural Gas Science and Engineering*, vol. 52, pp. 106–116, 2018.

[18] H. Y. Yu, Y. H. Zhang, M. Lebedev et al., "Nanoscale geomechanical properties of Western Australian coal," *Journal of Petroleum Science and Engineering*, vol. 162, pp. 736–746, 2018.

[19] C. L. Sun, G. C. Li, M. E. Gomah, J. H. Xu, and Y. T. Sun, "Creep characteristics of coal and rock investigated by nanoindentation," *International Journal of Mining Science and Technology*, vol. 30, no. 6, pp. 769–776, 2020.

[20] G. Manjunath and R. R. Nair, "Microscale assessment of 3D geomechanical structural characterization of gondawana shales," *International Journal of Coal Geology*, vol. 181, pp. 60–74, 2017.

[21] A. R. Sakulich and V. C. Li, "Nanoscale characterization of engineered cementitious composites (ECC)," *Cement and Concrete Research*, vol. 41, no. 2, pp. 169–175, 2011.

[22] S. Barbhuiya and B. Caracciolo, "Characterisation of asphalt concrete using nanoindentation," *Materials*, vol. 10, no. 7, p. 823, 2017.

[23] H. Lee, V. Vimonsatit, and P. Chindaprasirt, "Mechanical and micromechanical properties of alkali activated fly-ash cement based on nano-indentation," *Construction and Building Materials*, vol. 107, pp. 95–102, 2016.

[24] W. Li, B. Jiang, S. Gu, X. Yang, and F. Shaikh, "Experimental study on the shear behaviour of grout-infilled specimens and micromechanical properties of grout-rock interface," *Journal of Central South University*, vol. 2022, pp. 1–14, 2022.

[25] Y. Li, J. H. Yang, Z. J. Pan, and W. S. Tong, "Nanoscale pore structure and mechanical property analysis of coal: an insight combining AFM and SEM images," *Fuel*, vol. 260, p. 116352, 2020.

[26] Y. Li, Z. S. Wang, Z. J. Pan, X. L. Niu, Y. Yu, and S. Z. Meng, "Pore structure and its fractal dimensions of transitional shale: a cross-section from east margin of the Ordos Basin, China," *Fuel*, vol. 241, pp. 417–431, 2019.

[27] Y. B. Liu, G. Z. Yin, D. M. Zhang et al., "Directional permeability evolution in intact and fractured coal subjected to true-triaxial stresses under dry and water-saturated conditions," *International Journal of Rock Mechanics and Mining Sciences*, vol. 119, pp. 22–34, 2019.

[28] Y. L. Lu and L. G. Wang, "Effect of water and temperature on short-term and creep mechanical behaviors of coal measures mudstone," *Environmental Earth Sciences*, vol. 76, no. 17, p. 597, 2017.

[29] L. P. Li, C. S. Shang, K. W. Chu et al., "Large-scale geomechanical model tests for stability assessment of super-large cross-section tunnel," *Tunnelling and Underground Space Technology*, vol. 109, p. 103756, 2021.

[30] K. E. Eang, T. Igarashi, M. Kondo, T. Nakatani, C. B. Tabelin, and R. Fujinaga, "Groundwater monitoring of an open-pit limestone quarry: water-rock interaction and mixing estimation within the rock layers by geochemical and statistical analyses," *International Journal of Mining Science and Technology*, vol. 28, no. 6, pp. 849–857, 2018.

[31] P. L. P. Wasantha and P. G. Ranjith, "Water-weakening behavior of Hawkesbury sandstone in brittle regime," *Engineering Geology*, vol. 178, no. 8, pp. 91–101, 2014.

[32] B. Vásárhelyi and P. Ván, "Influence of water content on the strength of rock," *Engineering Geology*, vol. 84, no. 1-2, pp. 70–74, 2006.

[33] X. H. Wang, S. Jacobsen, J. Y. He, Z. L. Zhang, S. F. Lee, and H. L. Lein, "Application of nanoindentation testing to study of the interfacial transition zone in steel fiber reinforced mortar," *Cement and Concrete Research*, vol. 39, no. 8, pp. 701–715, 2009.

[34] W. Da Silva, J. Němeček, and P. Štemberk, "Methodology for nanoindentation-assisted prediction of macroscale elastic properties of high performance cementitious composites," *Cement and Concrete Composites*, vol. 45, pp. 57–68, 2014.

[35] S. H. Zhao, Y. Li, Y. B. Wang, Z. T. Ma, and X. Q. Huang, "Quantitative study on coal and shale pore structure and surface roughness based on atomic force microscopy and image processing," *Fuel*, vol. 244, pp. 78–90, 2019.

[36] K. Q. Liu, M. Ostadhassan, B. Bubach, K. G. Ling, B. Tokhmechi, and D. Robert, "Statistical grid nanoindentation analysis to estimate macro-mechanical properties of the Bakken Shale," *Journal of Natural Gas Science and Engineering*, vol. 53, pp. 181–190, 2018.

[37] C. L. Hu and Z. J. Li, "A review on the mechanical properties of cement-based materials measured by nanoindentation," *Construction and Building Materials*, vol. 90, pp. 80–90, 2015.

[38] M. Miller, C. Bobko, M. Vandamme, and F.-J. Ulm, "Surface roughness criteria for cement paste nanoindentation," *Cement and Concrete Research*, vol. 38, no. 4, pp. 467–476, 2008.

[39] G. Constantinides and F.-J. Ulm, "The nanogranular nature of C–S–H," *Journal of the Mechanics and Physics of Solids*, vol. 55, no. 1, pp. 64–90, 2007.

[40] J. Němeček, "Creep effects in nanoindentation of hydrated phases of cement pastes," *Materials Characterization*, vol. 60, no. 9, pp. 1028–1034, 2009.

[41] J. Xu, D. J. Corr, and S. P. Shah, "Nanomechanical investigation of the effects of nanoSiO2 on C–S–H gel/cement grain interfaces," *Cement and Concrete Composites*, vol. 61, pp. 7–17, 2015.

[42] G. Constantinides, K. S. R. Chandran, F. J. Ulm, and K. J. V. Vliet, "Grid indentation analysis of composite microstructure and mechanics," *Materials Science and Engineering A*, vol. 430, no. 1-2, pp. 189–202, 2006.

[43] Y. Li, J. Chen, J.-H. Yang, J.-S. Liu, and W.-S. Tong, "Determination of shale macroscale modulus based on microscale measurement: a case study concerning multiscale mechanical characteristics," *Petroleum Science*, 2021.

[44] F. J. Ulm, M. Vandamme, C. Bobko, J. Alberto Ortega, K. Tai, and C. Ortiz, "Statistical indentation techniques for hydrated nanocomposites: concrete, bone, and shale," *Journal of the American Ceramic Society*, vol. 90, no. 9, pp. 2677–2692, 2007.

[45] F. Zhang, H. Q. Guo, D. W. Hu, and J. F. Shao, "Characterization of the mechanical properties of a claystone by nano-

indentation and homogenization," *Acta Geotechnica*, vol. 13, no. 6, pp. 1395–1404, 2018.

[46] Y. H. Zhang, M. Lebedev, A. Al-Yaseri et al., "Nanoscale rock mechanical property changes in heterogeneous coal after water adsorption," *Fuel*, vol. 218, pp. 23–32, 2018.

[47] X. G. Zhang, P. Ranjith, Y. Y. Lu, and A. Ranathunga, "Experimental investigation of the influence of CO_2 and water adsorption on mechanics of coal under confining pressure," *International Journal of Coal Geology*, vol. 209, pp. 117–129, 2019.

[48] M. E. Broz, R. F. Cook, and D. L. Whitney, "Microhardness, toughness, and modulus of Mohs scale minerals," *American Mineralogist*, vol. 91, no. 1, pp. 135–142, 2006.

[49] T. Mori and K. Tanaka, "Average stress in matrix and average elastic energy of materials with misfitting inclusions," *Acta Metallurgica*, vol. 21, no. 5, pp. 571–574, 1973.